

Investigating Single-Crystal Rock Salt's Mechanical Behavior under Cyclic and Unloading-Reloading Loading Condition

Moslehy, A., Alshibli, K.A. and Truster, T.J.

Country Department of Civil and Environmental Engineering, University of Tennessee, Knoxville, TN, USA 37996, USA

Copyright 2021 ARMA, American Rock Mechanics Association

This paper was prepared for presentation at the 55th US Rock Mechanics/Geomechanics Symposium held in Houston, Texas, USA, 20-23 June 2021. This paper was selected for presentation at the symposium by an ARMA Technical Program Committee based on a technical and critical review of the paper by a minimum of two technical reviewers. The material, as presented, does not necessarily reflect any position of ARMA, its officers, or members. Electronic reproduction, distribution, or storage of any part of this paper for commercial purposes without the written consent of ARMA is prohibited. Permission to reproduce in print is restricted to an abstract of not more than 200 words; illustrations may not be copied. The abstract must contain conspicuous acknowledgement of where and by whom the paper was presented.

ABSTRACT: Gas storage caverns built within rock salt formations experience cyclic loading conditions either when gas is injected into the storage or when the gas is retrieved. The behavior of polycrystalline rock salt under cyclic loading conditions is well documented in the literature; however, single-crystal rock salt's behavior under cyclic loading is yet under-explored. This paper attempts to address this gap using cyclic and quasi-static loading-unloading tests on natural single-crystal specimens. Additionally, single-crystal rock salt's mechanical response is rather anisotropic; therefore, specimens with various crystal orientations are tested and evaluated. The specimens investigated in cyclic tests at 70%-80% of their unconfined compressive strength did not exhibit a significant change in their Young's modulus and damage parameters even after 30 cycles. However, the specimen tested on 30° to (1 0 0) in (0 1 0) direction showed a consistent increase in damage parameter with the number of cycles showing this crystal orientation is prone to fatigue damage.

1. INTRODUCTION

Rock salt is one of the prospective rock masses suitable for storing hazardous waste or various forms of energy (Hansen and Leigh, 2011; Marques et al., 2013; Titler et al., 2011; Urai et al., 1986). Rock salt can adapt to variation in the storage conditions such as pressure and temperature due to its low-permeability, ductile behavior, and self-healing properties in comparison to other rock formations (Chen et al., 2013; Yin et al., 2019). Rock salt formation may experience cyclic loading conditions either by natural periodic dynamic loads such as earthquakes or by applied cyclic service loads. A salt cavern experiences cyclic service loads when the pressure of the stored gas inside the cavern fluctuates due to gas injection or retrieval (Fuenkajorn and Phueakphum, 2010; Khaledi et al., 2016; Liang et al., 2012). Although the frequency of the cyclic service loads is significantly small, as normal retrieval or injection does not occur more than once a day, still, these loads are applied to the cavern time after time causing conditions similar to a traditional cyclic test (Voznesenskii et al., 2017). Therefore, studying the behavior of rock salt under cyclic loading conditions becomes intertwined with the serviceability of salt caverns.

Liu et al., 2014 investigated the evolution of rock salt under cyclic loading conditions. The polycrystalline

specimens containing a salt content of 84.8%-93.8% were obtained from a rock salt gas storage in Jintan city, Jiangsu Province, China. They found that only cyclic loads that are greater from 20%-40% of the uniaxial compressive strength of the tested rock can lead to fatigue damage development. Chen et al., 2016 evaluated the mechanical properties of Jintan city, Jiangsu Province, China rock salt under loading-unloading conditions at various confining stresses to simulate the condition of gas storages under service loads. The effect of confining pressure was determined to be minimal; additionally, the unloading-reloading loads did not influence the stressstrain curves of the specimens enough to deviate from the monotonic loading condition. Han et al., 2020 studied the effects of the mean stress, half-amplitude, and cycle period on cyclic behavior of polycrystalline rock salt to establish a modified creep model for predicting the timedependent deformation of rock salt. The steady strain rate and axial strain of the samples directly increased with increasing the three mentioned cycle parameters. Accelerated accumulation of damage with the samples was only observed after the samples had entered the tertiary creep deformation range.

As summarized above, the cyclic behavior of polycrystalline rock salt has been well studied. However, not all rock salt formations are polycrystalline, and even within polycrystalline rock salt formations the response of

rock salt single-crystals composing the formation heavily influences rock salt's cyclic response, which has not been reported in the literature. This paper investigates the behavior of single-crystal rock salt specimens with various crystal orientations (CO) under cyclic and quasistatic loading-unloading cycles.

2. SPECIMEN PREPARATION

The natural single-crystal rock salt specimens used in this study were sourced from Windsor Salt Mine, Ontario, Canada. Powder x-ray diffraction experiments on the source rock revealed a salt (NaCl) content of 99.9%. Cutting natural single-crystal rock salt specimens in a cylindrical shape is not easily achievable due to activation of {1 0 0} cleavage planes through the cutting process which results in breaking the specimen. Therefore, the single-crystal specimens were cut in cuboidal shapes with heights of about 30.0 mm and a width-to-height ratio of 1:2. The crystal orientations of the specimens prior to cut were approximated based on the orientation of the $\{1\ 0\ 0\}$ cleavage planes with specimen surfaces. The selected crystal orientations (CO) in this study were: parallel to [1 0 0] (abbreviated as 0° specimens), 19° to (1 0 0) in (0 1 0) (abbreviated as 19° specimens), and 30° to (1 0 0) in (0 1 0) (abbreviated as 30° specimens), which in the Bunge

Euler definition can be written as
$$\begin{bmatrix} \varphi_1 = 0 \\ \Phi = 0 \\ \varphi_2 = 0 \end{bmatrix}, \begin{bmatrix} \varphi_1 = 19^{\circ} \\ \Phi = 0 \\ \varphi_2 = 0 \end{bmatrix},$$

and
$$\begin{bmatrix} \varphi_1 = 30^{\circ} \\ \Phi = 0 \\ \varphi_2 = 0 \end{bmatrix}$$
, respectively. φ_1 is specimen axes'

counterclockwise rotation angles about the z-axis for transferring the specimen axes to the crystal axes, while Φ and φ_2 in order are specimen axes' counterclockwise rotation angles about the [1 0 0] and [0 0 1] directions for transferring the specimen axes to the crystal axes. 0° specimens tend to activate the $\{1 \ 1 \ 0\} < 1 \ -1 \ 0 > slip$ system under uniaxial compression since the Schmid factor on this direction is 1.0 and the critical resolved shear stress is much lower than other rock salt's slip systems. On the other hand, the $\{1\ 1\ 1\} < 1\ -1\ 0 > slip$ system has a higher chance to become active during the unconfined compression of 19° specimens due to the fact that its Schmid factor (1.2) is relatively greater than other slip systems at this crystal orientations. The crystal orientations of selected specimens were reevaluated using Laue x-ray diffraction experiments which confirmed all established crystal orientations. Two specimens of each selected crystal orientation were prepared for cyclic and quasi-static loading-unloading tests (Figure 1). Table 1 summarizes the initial physical properties of the specimens (specimens prepared for the cyclic tests are denoted with a "C' in Table 1, whereas the quasi-static loading-unloading specimens are denoted with "UR").

Table 1. Initial physical properties of the specimens

Specimen	СО	Height	Length	Width	Mass
		(mm)	(mm)	(mm)	(g)
C_0°	Parallel	30.2	16.5	15.8	16.90
UR_0°	to [1 0 0]	28.5	16.2	14.2	14.13
C_19°	19° to	29.9	17.0	14.4	15.63
UR_19°	(1 0 0) in (0 1 0)	26.8	18.3	13.7	14.57
C_30°	30° to	30.9	20.4	17.3	17.44
UR_30°	(1 0 0) in (0 1 0)	30.9	15.1	14.3	14.44

Table 2. Mechanical properties of the specimens after the tests

Specimen	$\sigma_{\rm y}$	$\sigma_{\rm c}$	E ₁	σ_{u}	ϵ_{u}
	(MPa)	(MPa)	(GPa)	(MPa)	(%)
C_0°	7.9	16.0	6.2	-	-
C_19°	9.5	17.9	6.0	-	-
C_30°	12.3	26.0	5.0	-	-
UR_0°	8.4	-	1.4	20.8	8.5
UR_19°	8.7	-	1.2	29.4	10.1
UR_30°	11.3	-	1.4	33.7	10.0

3. CYCLIC TESTS

One specimen of each crystal orientation was tested under cyclic loading conditions. The loads were applied to the specimens using a sine-wave with a frequency of 0.03 Hz and the total number of cycles was set to 30 cycles. The load amplitude (σ_c) was calculated to be in 70%-80 % of the unconfined compressive strength (σ_{ij}) of the material in each loading direction (Table 2). Figure 1d-f show the specimens after the tests. Compared to the pictures of the specimens before the tests (Figure 1a-c), many {1 0 0} planes are locally cleaved, and the 19° and 30° specimens illustrate some rotation in the lateral direction. However, with the exception of the 30° specimen, which showed local cleavage failure on the surface facing the camera at the end of the test, the specimens remained intact (one piece) at the end of the tests. The specimens' axial strain (ϵ_1) versus axial stress (σ_1) relationships are plotted in Figure 2. Figure 3a shows the specimens' calculated Young's moduli (E) at each cycle. The calculated E of all the specimens did not show any significant changes throughout the tests. The damage within the specimens can be estimated using Lemaitre's isotropic damage parameter (D) as defined in Eq. (1) (Lemaitre, 1985):

$$D = 1 - (1 - \frac{\epsilon_p}{\epsilon}) \frac{E'}{E} \tag{1}$$

where, ϵ_p is the specimen's irreversible strain at each step, ϵ is the specimen's total strain, E' is the damaged specimen's Young's modulus, and E is the intact specimen's Young's modulus. The evolution of D after each cycle is illustrated in Figure 3b. The damage occurring within the 0° and 19° specimens did not increase significantly after each cycle. The σ_c applied to the 0° and

 19° specimens was closer to 80% of σ_u in each direction, which has caused their *D* after the first cycle to be more than the 30° specimen whose σ_c was about 70% of σ_u in

this direction. On the other hand, the amount of damage occurred within the 30° specimen increased as the test progressed, which is a sign of fatigue damage accumulating within the specimen.

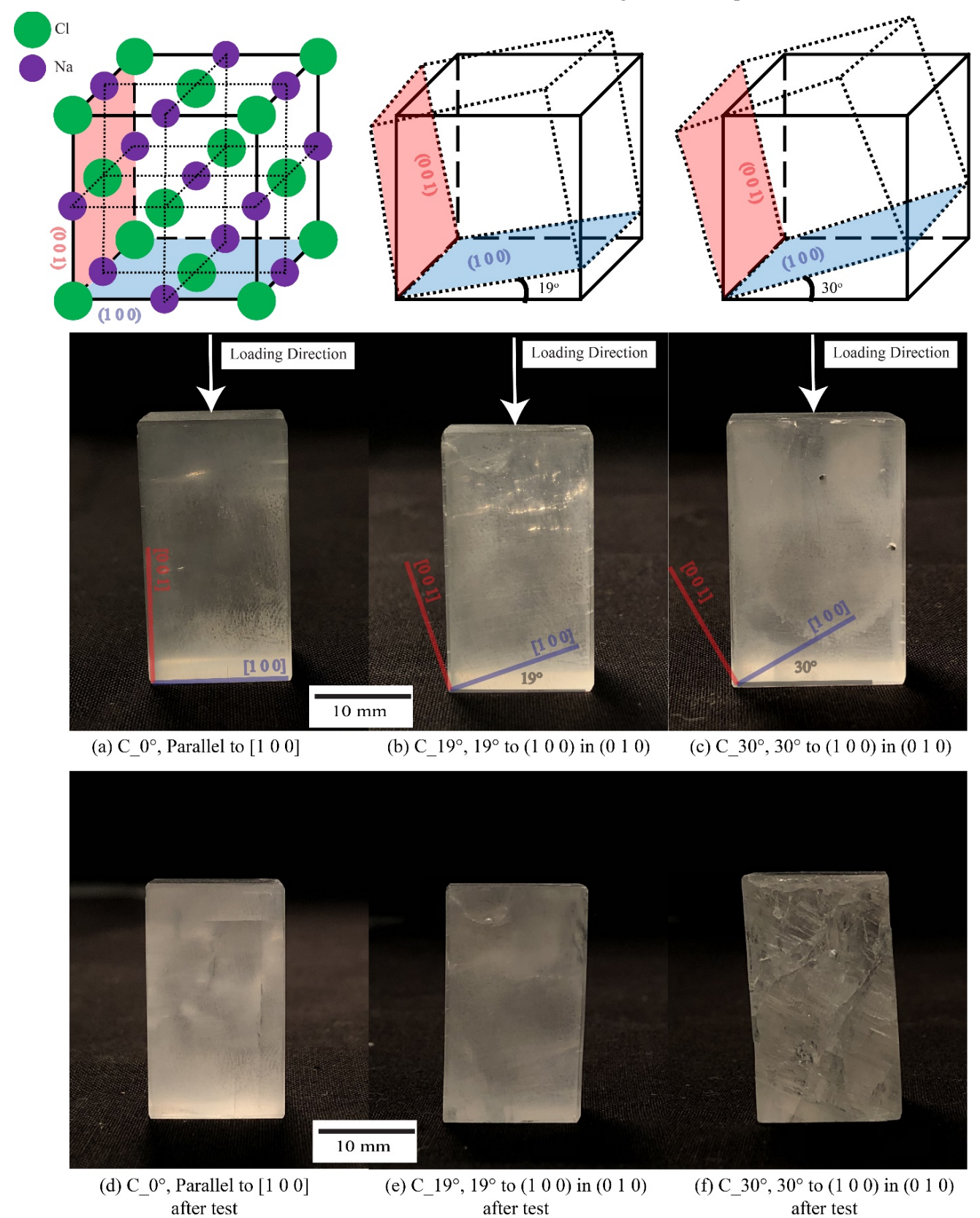


Figure 1. Cyclic test specimens (with various crystal orientations) before and after tests (loading-unloading specimens were prepared with similar crystal orientations)

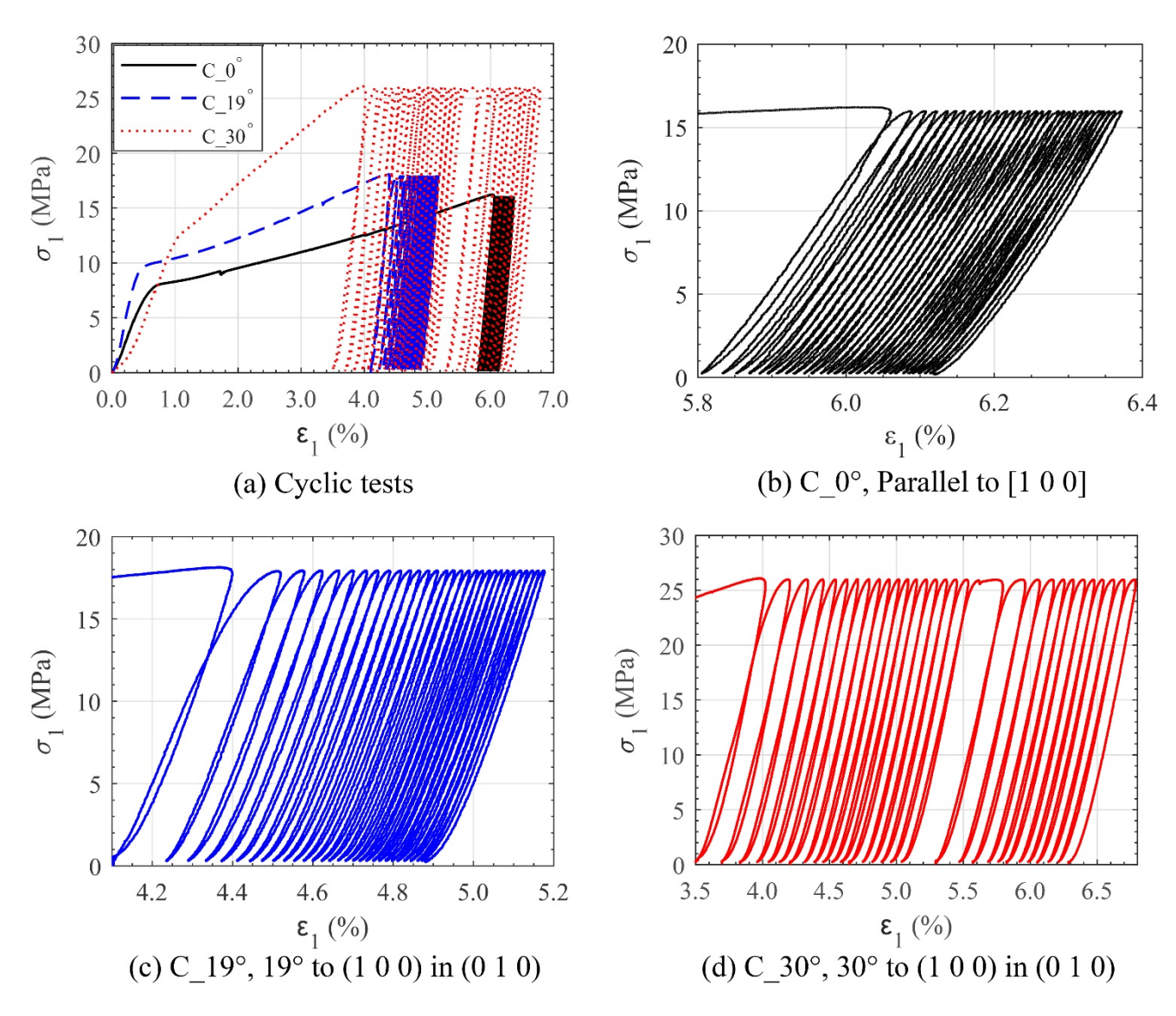


Figure 2. Cyclic test results on specimens loaded on various crystal orientations

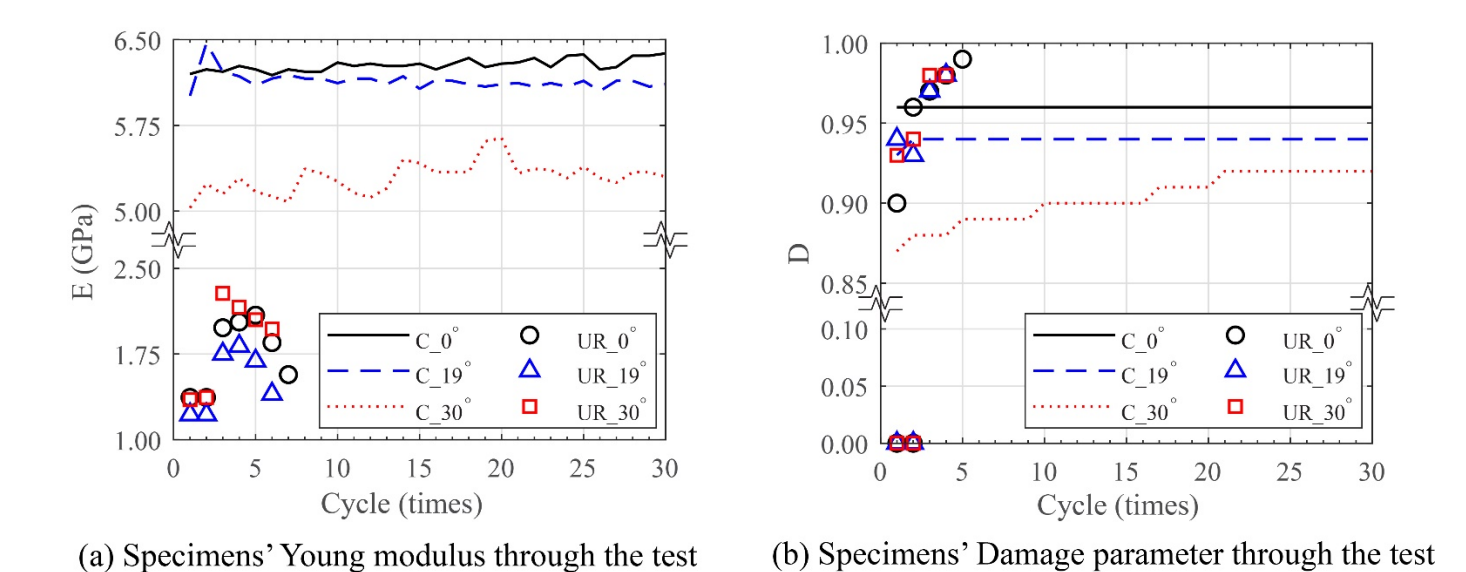
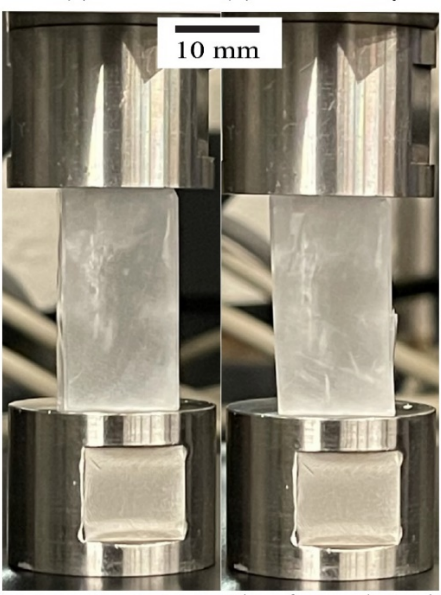
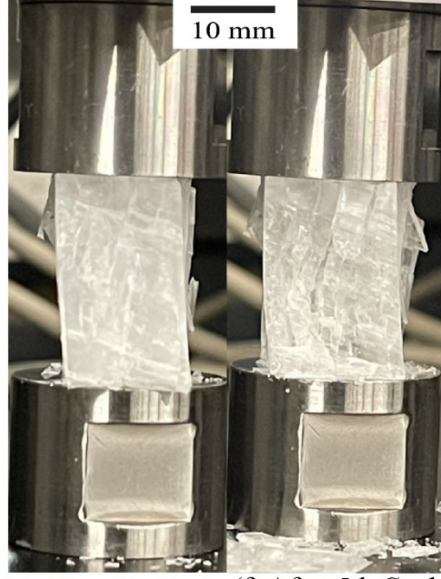


Figure 3. Young's modulus and damage parameter of the specimens through the tests





(c) After 2nd Cycle (d) After 3rd Cycle



(e) After 4th Cycle (f) After 5th Cycle

Figure 4. UR_19° specimen through the quasi-static loading-unloading cycles

4. QUASI-STATIC LOADING-UNLOADING TESTS

A specimen of each crystal orientation was tested under quasi-static loading-unloading condition. Both the loading and unloading cycles were applied using a constant strain rate of $1.7 \times 10^{-4} \, s^{-1}$. The following unloading-reloading cycles were applied to each specimen: one cycle before the material's yield stress ($\sigma_{\rm v}$) in each direction, two cycles after σ_v before reaching σ_u , one cycle near σ_u , and at least one cycle after reaching σ_u before the specimen's collapse. A summary of the mechanical properties of the specimens is reported in Table 2. Figure 4 shows UR 19° specimen throughout the test. Although a significant amount of the {1 0 0} cleavage planes became apparent before reaching σ_{ii} , no local failure was observed (Figure 4b-d). The specimens' ϵ_1 versus σ_1 relationships during the loading-unloading tests are depicted in Figure 5. The 19° specimen exhibited a higher σ_{ij} and axial strain at failure (ϵ_{ij}) than expected. Looking at Figure 4, the 19° specimen seems to have more locally activated {1 0 0} cleavage planes which can obstruct a cleavage failure forming throughout the specimen resulting in the specimen's unexpected behavior. The specimens' Young's moduli (E) and damage parameters (D) versus the cycle number are shown in Figure 3. Interestingly, all specimens' E increased when the applied stresses exceeded σ_v . However, as the experiments progressed, the specimens' E values were gradually decreased. On the other hand, none of the specimens showed any damage when stressed within their elastic ranges. Surpassing the σ_v in each direction, the specimens showed a consistent increase in damage after each unloading-reloading cycle.

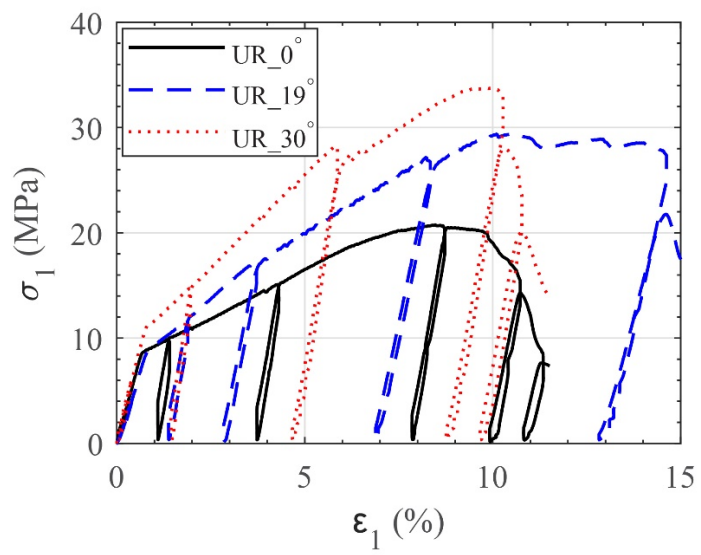


Figure 5. Quasi-static loading-unloading test results on specimens loaded on various crystal orientations

5. CONCLUSIONS

Cyclic and quasi-static loading uniaxial strength properties of single-crystal rock salt loaded on various crystal orientations were studied. The specimens tested in cyclic loading with load amplitudes of 70%-80% of the material's unconfined compressive strength in each direction did not show a significant change in their Young's modulus after 30 loading cycles. Moreover, the specimens loaded parallel to [1 0 0] and 19° to (1 0 0) in (0 1 0) did not exhibit an increased damage parameter at higher loading cycles. However, the specimen tested on 30° to (1 0 0) in (0 1 0) showed a steady gradual increase in damage parameter as the experiment progressed. The specimens tested using quasi-static loading-unloading procedure initially displayed a larger Young's modulus after surpassing their directional yield stresses followed with a consistent decrease as the stresses were increased to reach or surpass the specimens' unconfined compressive strength in each direction. The specimens did not manifest any damage prior to reaching the yield point. The damage parameters of the specimens increased after surpassing the directional yield stresses due to significant accumulation of plastic deformations.

ACKNOWLEDGMENTS

This material is based on work supported by the National Science Foundation (NSF) under Grant # CMMI-1641054. Any opinions, findings, conclusions, and recommendations expressed in this material are those of the authors and do not necessarily reflect the views of NSF. PXRD and LXRD were acquired at the Joint Institute for Advanced Materials (JIAM) Diffraction Facility of the University of Tennessee, Knoxville. The authors are grateful to Darcie Halliburton, an undergraduate research assistant at the University of Tennessee, Knoxville, for her help in preparing some of the specimens.

REFERENCES

Chen, J., C. Du, D. Jiang, J. Fan, and Y. He. 2016. The mechanical properties of rock salt under cyclic loading-unloading experiments. *Geomechanics and Engineering*. 10(3), 325–334.

Chen, J., S. Ren, C. Yang, D. Jiang, and L. Li. 2013. Self-healing characteristics of damaged rock salt under different healing conditions. *Materials*. 6(8), 3438–3450.

Fuenkajorn, K., and D. Phueakphum. 2010. Effects of cyclic loading on mechanical properties of Maha Sarakham salt. *Engineering Geology*. 112(1–4), 43–52.

Han, Y., H. Ma, C. Yang, N. Zhang, and J. J. K. Daemen. 2020. A Modified Creep Model for Cyclic Characterization of Rock Salt Considering the Effects of the Mean Stress, Half-Amplitude and Cycle Period. *Rock Mechanics and Rock Engineering*. 53(7), 3223–3236.

Hansen, F. D., and C. D. Leigh. 2011. Salt disposal of heat-generating nuclear waste. *Sandia National Laboratories Albuquerque, NM*.

Khaledi, K., E. Mahmoudi, M. Datcheva, and T. Schanz. 2016. Stability and serviceability of underground energy storage caverns in rock salt subjected to mechanical cyclic loading. *International Journal of Rock Mechanics and Mining Sciences*, 86, 115–131.

Lemaitre, J. 1985. A Continuous Damage Mechanics Model for Ductile Fracture. *Journal of Engineering Materials and Technology*. 107(1), 83–89. https://doi.org/10.1115/1.3225775

Liang, W., C. Zhang, H. Gao, X. Yang, S. Xu, and Y. Zhao. 2012. Experiments on mechanical properties of salt rocks under cyclic loading. *Journal of Rock Mechanics and Geotechnical Engineering*. 4(1), 54–61.

Liu, J., H. Xie, Z. Hou, C. Yang, and L. Chen. 2014. Damage evolution of rock salt under cyclic loading in uniaxial tests. *Acta Geotechnica*. 9(1), 153–160.

Marques, F. O., J.-P. Burg, M. Armann, and E. Martinho. 2013. Rheology of synthetic polycrystalline halite in torsion. *Tectonophysics*. 583, 124–130.

Titler, R. V, and P. Curry. 2011. Chemical analysis of major constituents and trace contaminants of rock salt. *Pennsylvania Department of Environmental Protection*.

Urai, J. L., C. J. Spiers, H. J. Zwart, and G. S. Lister. 1986. Weakening of rock salt by water during long-term creep. *Nature*. 324(6097), 554.

Voznesenskii, A. S., M. N. Krasilov, Y. O. Kutkin, M. N. Tavostin, and Y. V. Osipov. 2017. Features of interrelations between acoustic quality factor and strength of rock salt during fatigue cyclic loadings. *International Journal of Fatigue*. 97, 70–78.

Yin, H., C. Yang, H. Ma, X. Shi, X. Chen, N. Zhang, X. Ge, and W. Liu. 2019. Study on damage and repair mechanical characteristics of rock salt under uniaxial compression. *Rock Mechanics and Rock Engineering*. 52(3), 659–671.